 SDHM, vol.5, no.1, pp.33-55, 2009

# Real Time Damage State Estimation and Condition Based Residual Useful Life Estimation of a Metallic Specimen under Biaxial Loading

**S.Mohanty[1], A. Chattopadhyay[2], J. Wei[3] and P. Peralta[4]**

**Abstract:** The current state of the art in the area of real time structural health monitoring techniques offers adaptive damage state prediction and residual useful life assessment. The present paper discusses the use of an integrated prognosis model, which combines an on-line state estimation model with an off-line predictive model to adaptively estimate the residual useful life of an Al-6061 cruciform specimen under biaxial loading. The overall fatigue process is assumed to be a slow time scale process compared to the time scale at which, the sensor signals were acquired for on-line state estimation. The on-line state estimation model was based on correlation analysis, which is a type of non-parametric system identification approach. A new damage index is proposed, which is proportional to the cumulative damage state of the structure at any particular fatigue cycle. The on-line model regularly estimates the current damage state of the structure based on passive strain gauge signals. These damage states were used to update the slow scale off-line predictive model as it becomes available. The off-line predictive model is a probabilistic nonlinear regression model, which is based on a Bayesian statistics based Gaussian process approach. The off-line module adaptively updates the model parameters and recursively predicts the future states to provide real time residual useful life estimate.

**Keywords:** Structural Health Monitoring (SHM), Real time state estimation, Fatigue life prediction, Damage index, Gaussian process, Correlation analysis, Residual useful life estimation (RULE)

[1] Graduate Student, Mechanical and Aerospace Engineering, ASU, Tempe, AZ, USA.
[2] Fellow ASME, AIAA, Professor, Mechanical and Aerospace Engineering, ASU, Tempe, AZ, USA.
[3] Assistant Professor Research, Mechanical and Aerospace Engineering, ASU, Tempe, AZ, USA.
[4] Associate Professor, Mechanical and Aerospace Engineering, ASU, Tempe, AZ, USA.

## Nomenclature

**Fast scale variables**

| | |
|---|---|
| $m$ | Lag numbers |
| $\Delta t$ | $(= 1/f_f)$ Time interval |
| $T$ | Observation time |
| $M$ | No. of observation samples |
| $u(m)$ | Input measurement at lag $m$ |
| $y(m)$ | Output measurement at lag $m$ |
| $\nu(m)$ | Noise contribution at lag $m$ |
| $\gamma_{uy}(m)$ | Cross correlation coefficient at lag $m$ |

**Slow scale variables**

| | |
|---|---|
| $n$ | Damage level number (or damage instances) |
| (Note: In general $n$ is not same as number of fatigue cycles) | |
| $\tilde{n}$ | Number of damage levels after last on-line or fast scale data available |
| $\tilde{n}^*$ | After last fast scale data available, the number of damage level to damage state become critical |
| $N$ | Total no. of fatigue cycles |
| $N_0$ | Fatigue cycle at first on-line data available |
| $\Delta N$ | Fatigue cycles per each damage level increment |
| $\theta_n^{\vartheta}$ | Noise hyperparameter at $n^{th}$ level |
| $\theta_n^{p}$ | Process hyperparameter at $n^{th}$ level |
| $\theta_n^{w}$ | Input weighing hyperparameter at $n^{th}$ level |
| $\theta_n^{b}$ | Bias hyperparameter at $n^{th}$ level |
| $\mathbf{x}_n$ | Input vector at $n^{th}$ level |
| $a_n$ | Output damage index at $n^{th}$ level |
| $\mathbf{K}_n$ | Kernel matrix at $n^{th}$ level |
| $k(\mathbf{x}_i, \mathbf{x}_j)$ | Kernel function at $n^{th}$ level |

## 1 Introduction

On-line health monitoring and prognostics is emerging at the forefront of Condition based Maintenance (CBM) of critical structural systems giving rise to the term Prognostic Health Management (PHM). Whether it is a newly acquired or an aging aircraft fleet, the structural life ceiling of the fleet is defined from three distinct approaches: safe-life, fail-safe, and damage tolerant approaches. A detailed review of these approaches is presented by Iyyer, Sarkar, Merrill, and Phan (2007). With the safe-life approach, the retirement life of a component is defined by crack initia-

tion time derived from a full-scale component, or element fatigue test. In practice, however, the component is retired before the formation of a fatigue crack by using high safety factors on calculated crack initiation time because of inherent variability in both static and fatigue material properties as well as assumptions made in analytical models used to calculate crack initiation time. The fail-safe approach assumes an initial damage due to manufacturing flaws and its subsequent growth during service to detectable crack sizes. Service life in fail-safe structures can thus be defined as the time to a survivable detectable damage. The fail-safe approach requires inspections as part of the maintenance program, and these inspections are also specifically geared to find damages in identified critical components of the aircraft. In the case of the damage-tolerant approach, it assumes initial defects, however small they may be in critical structural elements, which will eventually grow in to large crack sizes. Service life is estimated through rigorous crack growth analysis both deterministic and stochastic. A majority of the deterministic crack growth analysis models are based on the approach followed by FASTRAN [Newman (1992)] or AFGROW [Harter (2003)] type crack growth model. It should be noted that these models are based on some empirical parameters, which have to be tuned for a particular application. In the case of stochastic life estimation, two different approaches are generally being used in industry and are continuously being improved by the stochastic life modeling research community. In the first technique, service life is based on the basic principles of Miner's damage accumulation criteria, and in the second technique the stochastic crack growth curves are obtained first, followed by estimation of the corresponding stochastic service life. Wu and Ni (2004) presented a stochastic crack growth model which can be used for stochastic life estimation of structures. In the case of damage accumulation type models, the recent work by Liu and Mahadevan (2007) on nonlinear fatigue damage accumulation rule and a stochastic S-N curve representation technique for predicting stochastic fatigue life under variable amplitude loading is noteworthy. In the above mentioned deterministic or stochastic approaches the damage tolerance and fatigue life predictions are obtained based on assumed structural flaws or on previous coupon test results regardless of whether the assumed structural flaw actually occurs during service (i.e., prognosis is made before diagnosis). In addition in a real life scenario, changing loading conditions and other environmental conditions such as change in humidity and temperature, leads to different crack growth parameters, compared to those originally found from coupon testing. Consequently, a large degree of conservatism is incorporated into structural designs due to these uncertainties. The current research in the area of on-line damage state estimation [Gupta and Ray (2007)], offers methodologies for adaptive damage state prediction and residual useful life assessment. The on-line state estimation model can be either a supervised or unsupervised model. In a supervised approach, the

model has to be trained for known damage cases based on previously conducted tests. The supervised model is difficult to implement in real-life conditions. This is because of the changing boundary conditions and noise levels (due to electrical connections), which may not be similar to the previously obtained data used for training the model. A detailed review on different SHM approaches is presented by Farrar and et. al. (2003, 2007). For real time damage monitoring and prognosis, there is also a need for an effective predictive model to forecasts the future state and the remaining life of the structure. The real time damage state information from the on-line state estimation model [Mohanty, Chattopadhyay, and Peralta (2008)] can be regularly fed to the off-line predictive model [Mohanty, Das, Chattopadhyay, and Peralta (2009)] to update the residual useful life estimation. The bearing failure predictive model presented by Billington, Zhang, Kurfess, Danyluk, and Liang (1999) is among the few earliest reported works on real time adaptive predictive models. However, their model is based on a linear covariance structure, which may not always be suitable for learning nonlinear damage growth dynamics. The present paper proposes a recursive Gaussian process predictive model, in which the model parameters are adaptively updated to predict the future states and residual useful life estimate. Unlike the covariance based structure, the Gaussian process [Gibbs (1997); MacKay (1998); Rasmussen and Williams (2006)] uses the kernel function. The kernel function is a multi-dimensional function that transfers the linearly inseparable information first to a high dimensional feature space, where the information can be linearly separable. In addition, in the present paper non-parametric system identification technique based correlation analysis [Ljung (1999)] approach is used to estimate the current damage state. The current damage state is estimated by correlating the real time sensor measurements obtained from two different strain gauges placed at two different locations on the structure. Once the damage state (in the form of a damage index) is estimated, it is fed to the Gaussian process off-line predictive model to forecast the future damage state and residual useful life estimate (RULE). The real time algorithm is validated on an Al-6061 cruciform specimen undergoing biaxial fatigue loading.

## 2 Theoretical Approach

The integrated prognosis model is an adaptive model that works in conjunction with real time sensor measurements. As shown in Fig. 1, the integrated prognosis architecture has two distinct sub modules, the on-line state estimator and the off-line state predictor. The on-line state estimator infers the current state of the structure from real time sensor measurements. Once the current state information becomes available, it is fed to the off-line predictive model to predict the future states and the corresponding residual useful life is estimated. The estimated current state up-

date the initial condition of the predictive model. It is noted that the overall fatigue loading history is assumed to be a slow time scale process [Gupta and Ray (2007)] compared to the time scale at which the sensor signals are acquired. From this point onwards, the sensor signal acquiring process and corresponding current cycle damage state (or damage index) estimation process is denoted a fast scale process, whereas the overall slower fatigue process is denoted a slow scale process. It is noted that the fast scale sensor measurements are performed at discrete slow scale intervals. Also, at the individual slow scale instances, where the fast scale sensor measurements are acquired, the damage state of the structure is assumed to remain unchanged.

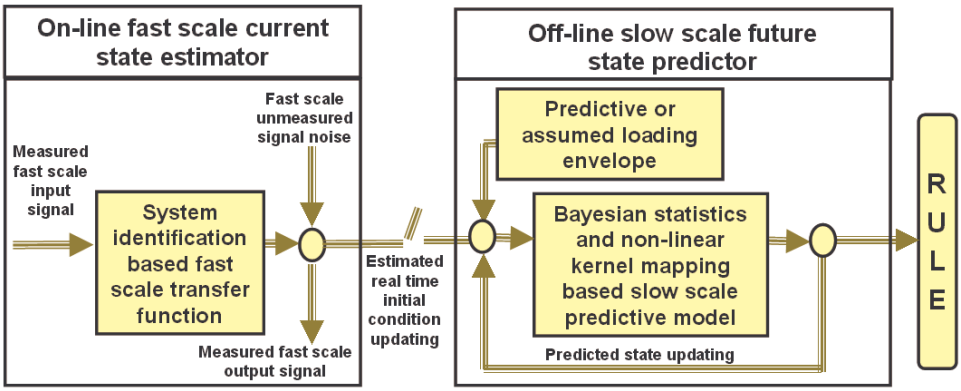


Figure 1: Schematic of an adaptive prognosis model.

## *2.1 On-line fast-scale damage state estimation*

### *2.1.1 Fast-scale transfer function estimation*

At any particular damage level, the output sensor measurement can be mapped with the input sensor measurement over a time invariant transfer function. It is noted that as the state of the structure changes, the input-output mapping becomes time variant and the corresponding transfer function has to be estimated recursively. A typical $n^{th}$ damage level block diagram that maps the input sensor measurements with the output sensor measurements is shown in Fig. 2. The fast scale z-domain transfer function $P(z)$ between input $u$ and output $y$ at $n^{th}$ damage level can be represented as:

$$\begin{aligned} y(t) &= P_n(z)u(t) + v(t) \\ &= (b_0 + b_1 z^{-1} + b_2 z^{-2} + \ldots + b_M z^{-M})u(t) + v(t) \end{aligned} \quad (1)$$

where $z^{-m}; m = 0, 1, \ldots M$ are the backspace operators of the pulse transfer function $P(z)$ and $b_m; m = 0, 1, \ldots M$ are the finite impulse response (FIR) coefficients. Eq. 1 can be rewritten in the discrete domain as

$$y(t) = b_0 u(t) + b_1 u(t-1) + b_2 u(t-2) + \ldots + b_M u(t-M) + v(t) \tag{2}$$

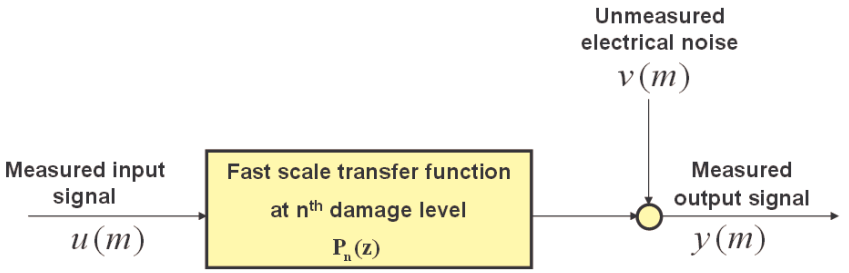


Figure 2: Block diagram for fast scale transfer function. The transfer function is an instantaneous representation of the time degrading structure at any typical damage level. However as the damage grow the transfer function also changes leading to a time variant approach of system identification.

### 2.1.2 Damage index

The slow scale damage index $a_n$, is the representative damage state inferred from $n^{th}$ damage level fast-scale sensor measurements. The damage index can be derived by evaluating the $m^{th}$ lagged output $y(t+m)$ from Eq. 2 and pre multiplying the input $u(t)$, obtaining

$$\begin{aligned} u(t)y(t+m) &= b_0 u(t)u(t+m) + b_1 u(t)u(t-1+m) \\ &+ b_2 u(t)u(t-2+m) + \ldots \\ &+ b_M u(t)u(t-M+m) + u(t)v(t+m) \end{aligned} \tag{3}$$

Applying expectation operator to both sides of Eq. 3 and assuming independence between noise and the input signal, the $m^{th}$ lagged cross-correlation coefficients can be expressed as

$$\begin{aligned} \gamma_{uy}(m) &= b_0 \gamma_u(m) + \gamma_u(m-1) + b_2 \gamma_u(m-2) + \ldots \\ &+ b_M \gamma_u(m-M); \quad m = 0, 1 \ldots, M \end{aligned} \tag{4}$$

With known input (u) and output (y) time series, the $m^{th}$ lagged cross-correlation coefficients $\gamma_{uy}(m)$ and auto-correlation coefficients $\gamma_u(m)$, the FIR coefficients $b_m; m = 0,1,\ldots M$ can be estimated. To estimate $M+1$ FIR coefficients we need to solve $M+1$ algebraic equations given by Eq. 4. However, solving $M+1$ algebraic equations involves inverting a $(M+1)\times(M+1)$ autocorrelation coefficient matrix, which becomes computationally expensive in the context of real time applications. To circumvent this problem the damage state equivalent damage index can be estimated. Based on the cross-correlation coefficients $\gamma_{uy}(m)$ a new damage index is formulated, which is expressed as follows:

$$a_n = \sqrt{\frac{\sum_{m=0}^{m=M}(\gamma_{uy}^n(m)-\gamma_{uy}^0(m))^2}{\sum_{m=0}^{m=M}(\gamma_{uy}^0(m))^2}}; \quad n = 1,2\ldots,N/\Delta N \tag{5}$$

where $\gamma_{uy}^n(m)$ represents $n^{th}$ damage level cross-correlation coefficients, and $\gamma_{uy}^0(m)$ represents reference condition cross-correlation coefficients.

## 2.2 *Off-line slow-scale damage state prediction and residual useful life estimation*

### 2.2.1 *Predicting in a Bayesian framework*

The goal of a probabilistic Bayesian forecasting approach is to compute the posterior distribution of a future damage state or damage index $a_{n+1}$, i.e., to determine the probability distribution of the random damage index $a_{n+1}$ given a random test input $\mathbf{x}_{n+1}$ and a set of $n$ training data points described as $D = \{\mathbf{x}_i, a_i\}_{i=1,\ldots,n}$. In the Bayesian framework, the predictive distribution with mean and variance can be found by conditioning the damage indices $a_1$, $a_2$,.....,$a_n$,$a_{n+1}$ that are affected by the corresponding random inputs $\mathbf{x}_1$, $\mathbf{x}_2$,.....,$\mathbf{x}_n$,$\mathbf{x}_{n+1}$. A prior over the space of possible functions to model the random damage index as $f(a_i|\alpha; i = 1,2,\ldots,n+1)$, can be defined where $\alpha$ are some hyperparameters that can account for random load sequence effect in the form of curve fitting. Also, a prior over the noise $f(\vartheta|\beta)$, can be defined where $\vartheta$ is some appropriate noise vector that arises due to scatter in material micro structure and $\beta$ is another set of hyperparameters used to model the uncertainty due to scatter. Now if the hyperparameters $\alpha$ and $\beta$ are given, the conditional probability [Rasmussen and Williams (2006)] can be expressed as

$$f(\mathbf{a}_{n+1}|\{\mathbf{x}_{i=1,\cdots,n},\alpha,\beta\}) = \int (\mathbf{a}_{n+1}|\{\mathbf{x}_{i=1,\cdots,n},a,\vartheta\})\, f(a|\alpha) f(\vartheta|\beta) da d\vartheta \tag{6}$$

where $a$ and $\vartheta$ denotes the underlying function which respectively corresponds to damage index and noise due to scatter. Since $a_1$, $a_2$,.....,$a_n$, and $a_{n+1}$ are conditioned random variables in the observed set of damage indices, the conditional

distribution of $a_{n+1}$ can be written as follows

$$f\left(a_{n+1}|D=\{\mathbf{x}_i,a_i\}_{i=1,\ldots,n},\mathbf{x}_{n+1},\alpha,\beta\right)=\frac{f\left(\mathbf{a}_{n+1}|\{\mathbf{x}_i\}_{i=1,\ldots,n+1},\alpha,\beta\right)}{f\left(\mathbf{a}_n|\{\mathbf{x}_i\}_{i=1,\ldots,n},\alpha,\beta\right)} \tag{7}$$

### 2.2.2 Predicting with a Gaussian process

To evaluate Eq. 7 it is necessary to evaluate the integral given in Eq. 6. However, in general, Eq. 6 is complicated to evaluate. The standard approach to evaluate the integral in Eq. 6 is by a method called evidence maximization [MacKay (1992)] or by numerically integrating by Monte Carlo simulation [Neal (2003)]. However, assuming the underlying damage index function $a_i$ follows a Gaussian distribution, the exact analytical form of Eq. 7 is as follows

$$f\left(\mathbf{a}_{n+1}|\{x_i\}_{i=1,\cdots,n},\mathbf{K}_{n+1}\right) = \frac{1}{(2\pi)^{n+1/2}det(\mathbf{K}_{n+1})^{1/2}}exp\left(-\frac{1}{2}(\mathbf{a}_{n+1}-\mu)^T\mathbf{K}_{n+1}^{-1}(\mathbf{a}_{n+1}-\mu)\right) \tag{8}$$

where $\mu$ is the function mean and $\mathbf{K}_n$ is a $n\times n$ kernel matrix. The individual elements $k$ of the kernel matrix $\mathbf{K}_n$ can be found from a parameterized kernel function that will be described in the next section. Assuming zero mean function distribution Eq. 8 can be written as

$$\begin{aligned} f(a_{n+1}|D &= \{\mathbf{x}_i,a_i\},\mathbf{x}_{n+1},k_{ij}(x_i,x_j,\Theta)_{i,j=1,2,..n}) \\ &= \sqrt{\frac{det(\mathbf{K}_n)}{(2\pi)det(\mathbf{K}_{n+1})}}exp(-\frac{(a_{n+1}-\hat{a}_{n+1})^2}{2\sigma^2_{\hat{a}_{n+1}}}) \end{aligned} \tag{9}$$

where $\hat{a}_{n+1}$ is the one-step ahead predicted mean at slow scale damage level $n+1$ and is given by

$$\hat{a}_{n+1}=\mathbf{k}^T\mathbf{K}_n^{-1}\mathbf{a}_n;\ \ k_i=k(\mathbf{x}_{n+1},\mathbf{x}_i)_{i=1,2,\ldots n} \tag{10}$$

$\sigma^2_{\hat{a}_{n+1}}$ is the one-step ahead predicted variance at slow scale damage level $n+1$ and is given by

$$\sigma^2_{\hat{a}_{n+1}}=\kappa-\mathbf{k}^TK_n^{-1}\mathbf{k};\ \ k_i=k(\mathbf{x}_{n+1},\mathbf{x}_i)_{i=1,2,\ldots n};\ \ \kappa=k(\mathbf{x}_{n+1},\mathbf{x}_{n+1}) \tag{11}$$

### 2.2.3 Parameterizing the kernel function

There are many possible choices of prior interpolating kernel functions. From a modeling point of view, the objective is to specify a prior kernel function that contains our assumptions about the structure of the process being modeled. Formally, it is required to specify a function that will generate a positive definite kernel matrix for any set of inputs. In this paper, a multi layer perceptron (MLP) [Williams (1997)] based kernel function is used, which has the following form

$$k(\mathbf{x}_i,\mathbf{x}_j,\Theta)=\theta_n^p Sin^{-1}\frac{\mathbf{x}_i^T\theta_n^w\mathbf{x}_j+\theta_n^b}{\sqrt{(\mathbf{x}_i^T\theta_n^w\mathbf{x}_i+\theta_n^b+1)(\mathbf{x}_n^T\theta_n^w\mathbf{x}_n+\theta_n^b+1)}}+\theta_n^{\vartheta} \tag{12}$$

In Eq. 12 the superscript $n$ represents the $n^{th}$ damage instances. It is noted that unlike the fixed hyperparameters, the hyperparameters in Eq. 12 are found adaptively as new data becomes available.

### 2.2.4 Hyperparameters determination

So far only properties of the prediction model for fixed values of the hyperparameters have been considered. This section discusses how to obtain the hyperparameters $\Theta$ for a fixed training data set $D=\{\mathbf{x}_i,a_i\}_{i=1,\ldots,n}$. Ideally integration over all possible hyperparameters should be done in order to obtain the best possible predictions of the function value $a_{n+1}$ at damage level $n+1$. Therefore,

$$f(a_{n+1}|D,\mathbf{x}_{n+1},K(\cdot))=\int f(a_{n+1}|D,\mathbf{x}_{n+1},K(\cdot),\Theta)\,f(\Theta|D,K(\cdot))\,d\Theta \tag{13}$$

The above integral is as complex as the integral given in Eq. 6 and also difficult to evaluate for a complex problem with several hyperparameters and a multiple input space. Out of the two possible approaches e.g., the Maximum evidence [MacKay (1992)] and the Monte Carlo [Neal (2003)] approach only the use of the maximum evidence approach will be discussed to evaluate the integral. Using maximum evidence approach, Eq. 13 can be written in its approximate form as

$$f(a_{n+1}|D,\mathbf{x}_{n+1},K(\cdot))\cong f(a_{n+1}|D,\mathbf{x}_{n+1},K(\cdot),\Theta_{MAP}) \tag{14}$$

The approximation in Eq. 14 is based on the assumption that the posterior distribution over $\Theta$, i.e $f(\Theta|D,K(\cdot))$, has a sharp peak around $\Theta_{MAP}$. This approximation is generally reasonable [Gibbs (1997)] and predictions are often found very close to those obtained using the true predictive distribution. Now to find the peak location of $f(\Theta|D,K(\cdot))$ the posterior distribution needs to be optimized , which can be written as

$$f(\Theta|D,K(\cdot))=\frac{f\left(\mathbf{a}_n|\{\mathbf{x}_i\}_{i=1,2,\ldots n},K(\cdot),\Theta\right)f(\Theta)}{f\left(\mathbf{a}_n|\{\mathbf{x}_i\}_{i=1,2,\ldots n},K(\cdot)\right)} \tag{15}$$

In Eq. 15, the denominator is independent of $\Theta$ and can be ignored in the optimization process. On the other hand, the other two terms, the likelihood $f(\mathbf{a}_n|\{\mathbf{x}_i\}_i, K(\cdot), \Theta)$, and the prior $f(\Theta)$, need to be considered in the optimization of $f(\Theta|D, K(\cdot))$. With the assumption that all damage indices $a_i$ follow a Gaussian distribution and using Eq. 8, the logarithm of the objective function can be written as

$$\begin{aligned} L &\equiv Log\left(f(\Theta|D, K(\cdot))\right) \\ &= -\frac{1}{2}Log(detK_n) - \frac{1}{2}\mathbf{a}_n^T K_n^{-1}\mathbf{a}_n - \frac{n}{2}Log(2\pi) + Logf(\Theta) \end{aligned} \tag{16}$$

The log-likelihood function $L$ in Eq. 16 is generally multi-modal and can be optimized using any multi-variate optimization algorithm. In the present work, the conjugate gradient method is used to optimize the log-likelihood function and to obtain the optimized hyperparameters. Note that it is common practice [Gibbs (1997)] to ignore the log prior term in Eq. 16 due to the absence of knowledge on $\Theta$. The resulting solution may not always a realistic solution, however it can be assumed that $Logf(\Theta)$ is implicitly modeled through the optimization of the log-likelihood $L$.

### 2.2.5 Input-output data set for single step ahead prediction

For single step ahead prediction, the Gaussian process prediction model given by Eq. 8, predicts the single step ahead damage index. For prediction of the $n+1^{th}$ damage index, the training data set $D$ and test input vector $\mathbf{x}_{n+1}$ can be stated as,

$$D = \left[\begin{array}{c|c} \mathbf{x}_i & a_i \end{array}\right]_{i=d,\ldots,n} = \left[\begin{array}{cccc} \overbrace{a_0 & a_1 & \ldots & a_{d-1}}^{Training\ data\ matrix} & \overbrace{a_d}^{Target\ vector} \\ a_1 & a_2 & \ldots & a_d & a_{d+1} \\ \vdots & \vdots & \ldots & \vdots & \vdots \\ a_{n-d} & a_{n-d+1} & \ldots & a_{n-1} & a_n \end{array}\right] \tag{17}$$

$$\mathbf{x}_{n+1} = \left[\begin{array}{cccc} \overbrace{a_{n-d+1} & a_{n-d+2} & \ldots & a_n}^{Test\ input\ data\ vector} \end{array}\right] \tag{18}$$

where in Eq. 17 and 18 the subscript $n$ symbolizes the $n^{th}$ damage instance or damage level, up to which the last on-line data was available, and $d$ symbolizes dimension of the input space.

### 2.2.6 Input-output data set for multi step ahead prediction

For multi step ahead prediction, the GP model given by Eq.8 recursively predicts the future state after the last on-line data available. However, unlike the single step ahead prediction model, the multi step ahead training data set $D$ and test input vector $\mathbf{x}_{n+\tilde{n}}$ are adaptively updated with off-line predicted damage indices rather than on-line estimated damage indices. For prediction of the $n+\tilde{n}^{th}$ damage index the training data set $D$ and test input vector $\mathbf{x}_{n+\tilde{n}}$ can be written as

$$
\begin{aligned}
D &= \left[ \mathbf{x}_i \mid a_i \right]_{i=d,\ldots,n-1+\tilde{n}} \\
&= \left[ \begin{array}{cccc|c}
\multicolumn{4}{c|}{\overbrace{\textit{Training data matrix}}} & \overbrace{\textit{Target vector}} \\
a_0 & a_1 & \ldots & a_{d-1} & a_d \\
a_1 & a_2 & \ldots & a_d & a_{d+1} \\
\vdots & \vdots & \ldots & \vdots & \vdots \\
a_{n-d} & a_{n-d+1} & \ldots & a_{n-1} & a_n \\
a_{n-d+1} & a_{n-d+2} & \ldots & a_n & a^p_{n+1} \\
a_{n-d+2} & a_{n-d+3} & \ldots & a^p_{n+1} & a^p_{n+2} \\
\vdots & \vdots & \ldots & \vdots & \vdots \\
a^p_{n-d-1+\tilde{n}} & a^p_{n-d+\tilde{n}} & \ldots & a^p_{n-2+\tilde{n}} & a^p_{n-1+\tilde{n}}
\end{array} \right]
\end{aligned}
\tag{19}
$$

$$
\mathbf{x}_{n+\tilde{n}} = \left[ \begin{array}{cccc}
\multicolumn{4}{c}{\overbrace{\textit{Test input data vector}}} \\
a^p_{n-d+\tilde{n}} & a^p_{n-d+\tilde{n}+1} & \ldots & a^p_{n-1+\tilde{n}}
\end{array} \right]
\tag{20}
$$

where in Eq. 19 and 20 the subscript $n$ symbolizes the damage instance up to which the last on-line data is available, and the subscript $\tilde{n}$ symbolizes the damage instance number after the last on-line data available, and the superscript $p$ symbolizes predicted damage index from the off-line module, as opposed to being estimated from the on-line model.

### 2.2.7 Residual useful life estimation (RULE)

The residual useful life estimation can be defined as the difference between the number of fatigue cycles at which the predicted damage index becomes critical, i.e reaches its critical value ($a^*$), and the number of fatigue cycles at which the last on-line data is available. The RULE can be defined as:

$$
RULE = (n+\tilde{n}^*)\Delta N + N_0 - (n)\Delta N - N_0 = \tilde{n}^*\Delta N \tag{21}
$$

where $\Delta N$ is the number of fatigue cycle increments per each increment of damage instance and $\tilde{n}^*$ corresponds to the number of damage instances for the damage index to become critical after the last available on-line data.

## 3 Numerical Results

### *3.1 Fatigue experiment and data collection*

To numerically validate the integrated prognosis algorithm, a fatigue test was performed on an Al-6061 cruciform specimen under biaxial loading. The loaded cruciform specimen in an MTS biaxial fatigue test frame can be seen in Fig.3. The specimen was subjected to a constant amplitude fatigue loading with maximum amplitude ($\sigma_{max}$) 4 kips and load ratio $R = 0.1$, and the biaxial machine actuator was operated with a frequency of 10 Hz. It should be noted that, the maximum stress amplitude was equal to two thirds the yield stress $\sigma_Y$. Based on nonlinear finite element analysis of cruciform specimen, the yield stress was approximated as $\sigma_Y = 6kips$. Also note that both the x-axis actuator and y-axis actuator of the biaxial frame were subjected to in-phase fatigue loading. For on-line state estimation, passive strain gauge sensors were used. Two strain gauges were mounted on the web area (Fig. 4a), one strain gauges mounted on the horizontal flange (Fig. 4b), and the other one on the vertical flange (Fig. 4b) of the cruciform specimen. In addition, a hole in the center of the specimen was made to create crack initiation in the web area of cruciform specimen. To accelerate damage growth an EDM notch of 1 mm length was made at left bottom quadrant boundary of the central hole ($45^o$ to the vertical axis). A 48 channel NI PXI system was used to collect the strain gauge signals and the measurements from the biaxial machine load cells. In addition, a high resolution SONY camera was used to visually monitor the crack growth. The data acquisition system and the computer capturing the visual image were synchronized with the biaxial machine controller to collect the time synchronized data/ image at a specified interval of $\Delta N = 1500cycles$. The data and image collection started at approximately 11 k cycles. The image and sensor data were collected at 47 different time instance. For the first 44 instances, the signals and images were collected while the biaxial machine was running and during the last three instances the data was collected when the machine was not running. This leads to a total of 44 different damage cases with the last damage state occurring at 75.5 kcycles. The proposed MATLAB based prognosis algorithm was also synchronized with the data acquisition system to estimate the current damage state, and to predict the future damage state and remaining useful life in real time.

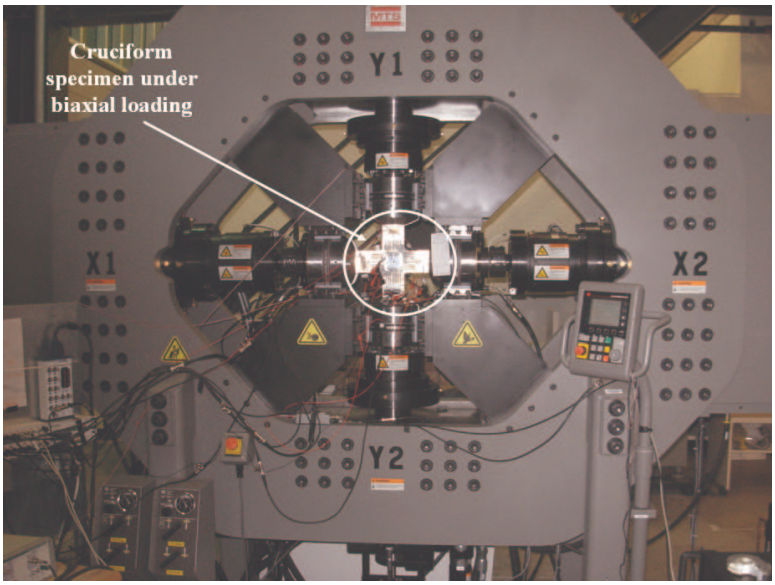


Figure 3: Al-6061 cruciform specimen loaded in a MTS biaxial fatigue test frame.

### *3.2 Correlation analysis based damage index estimation*

To evaluate the damage index as mentioned earlier, strain gauge measurements were mapped as input and output. For example, the signal ($\varepsilon_x^F$) from the strain gauge mounted on the horizontal flange (or X-arm) of the cruciform specimen was considered as the input signal $u$, whereas the signal ($\varepsilon_x^W$) from the web mounted stain gauge was considered as output $y$. It should be noted that both the horizontal axis strain ($\varepsilon_x^W$) and the vertical axis strain ($\varepsilon_y^W$) were measured by two different strain gauges placed perpendicular to each other. Comparison of input strain ($\varepsilon_x^F$) and output strain ($\varepsilon_x^W$) at different damage level are shown in Fig. 5. The figure shows the comparison for four different damage cases, damage case 7 (at 20 kcycle), damage case 20 (at 39.5 kcycle), damage case 42 (at 72.5 kcycle) and damage case 44 (at 75.5 kcycle). From the figure it can be seen that there is no clear trend between input and output strain at different damage levels. Rather than directly using the time series data for different damage case comparisons, using Eq. 4, the cross-correlation coefficient between input and output was found for different damage cases. The comparison of cross-correlation coefficients for damage level 1 (reference case at 11 k cycles) with cross-correlation coefficient at different damage levels are shown in Fig. 6. Figure 6a, 6b, 6c, and 6d, respectively show the comparison of cross-correlation coefficients of damage case 1 with damage case 7,

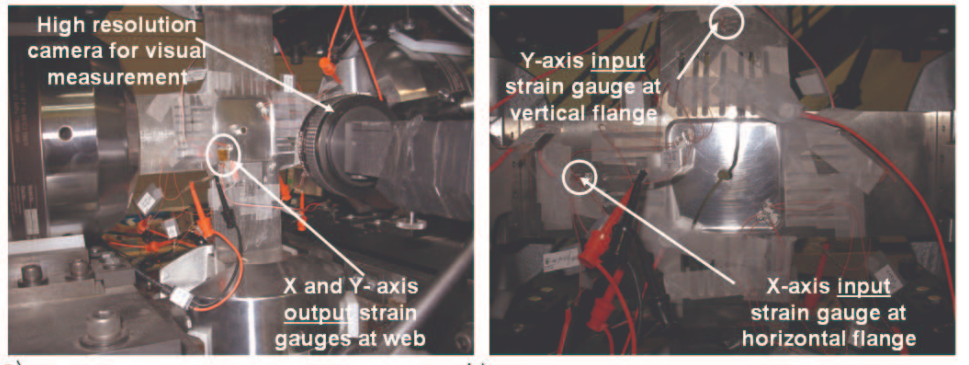


Figure 4: Undamaged and damaged condition of cruciform specimen: Fig. a shows the undamaged cruciform specimen. This rear view of the specimen also shows the location of two strain gauges mounted in the web area. Fig. b shows the final damage condition (at 75.5 kcycles) of the cruciform specimen. This front view of the specimen also shows the location of two strain gauges: one mounted on horizontal arm and the other mounted on the vertical arm of the specimen.

damage case 20, damage case-42 and damage case-44. It is to be noted that the results shown in Fig.6, the x-axis flange strain ($\varepsilon_x^F$) and x-axis web strain $\varepsilon_x^W$) are respectively taken as input $u$ and output $y$. Also, from Fig.6 it can be seen that the cross-correlation plot shows a better trend of damage growth, compared to the direct time series measurements shown in Fig. 5. However, to compare the quantitative damage states between different damage levels, the scalar damage index proposed in Eq. 5, was evaluated for the different damage states. Figure 7 shows the damage indices evaluated for two different output measurements, $\varepsilon_x^W$ and $\varepsilon_y^W$, against input measurements $\varepsilon_x^F$ from horizontal (x-axis) flange starain gauge. The figure shows a clear trend of damage growth with $\varepsilon_x^W$ as output strain compared to $\varepsilon_y^W$ as output strain. This is because the input signal $\varepsilon_x^F$ is poorly correlated with the y-axis web strain ($\varepsilon_y^W$) measurements. Figure 7 also shows that with respect to $\varepsilon_y^W$ as the output strain, except for final failure regime, there was no clear trend in damage growth. The higher damage indices during the final failure regime are possibly due to presence of shear strain components. Also from Fig. 7 a good correlation between normalized visual measurements and estimated damage indices (found with respect to $\varepsilon_x^W$ as output) is also observed. It must be noted that, the visual measurement is available up to damage level 29 (up to 53 kcycle). After the $29^{th}$ damage level, it was found that the camera went out of focus. In addition to

the strain signal as input, damage indices were also obtained using biaxial frame load cell measurements (x-axis load cell). The corresponding damage indices are shown in Fig. 8, and a similar trend in damage index growth, as in the previous case (with x-axis flange strain measurement as input), can be observed. However, it is noted that in a real life scenario, it is hardly possible to directly measure the loads applied to the structure. On the other hand, it is realistic to mount strain gauges or small sensors at required locations without affecting the structural integrity of the host structure. Therefore the results presented in the subsequent sections are based only on the strain gauge based data.

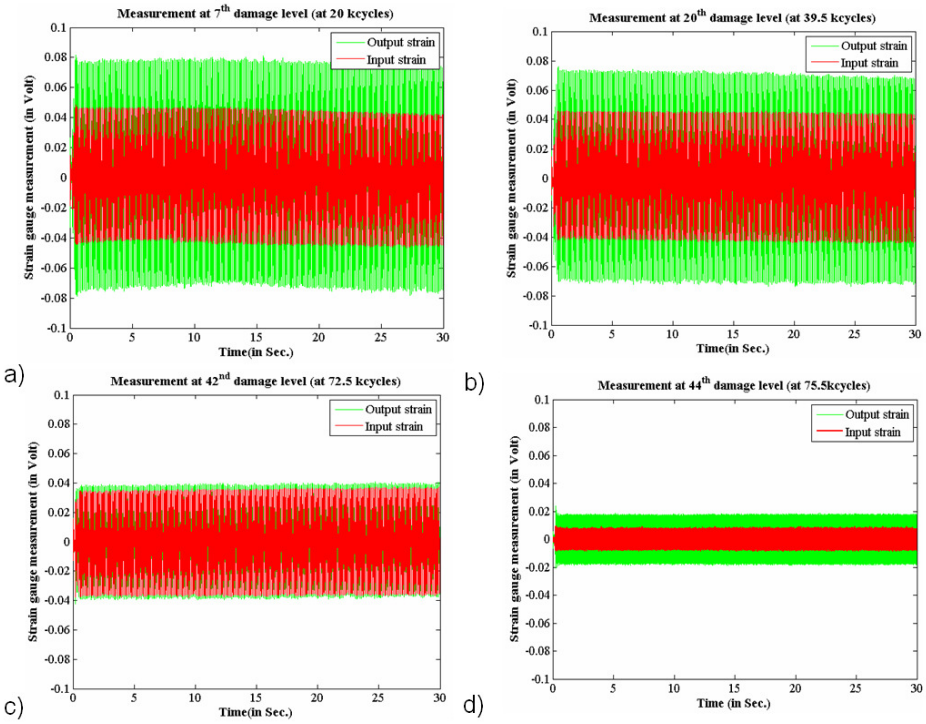


Figure 5: Input output strain comparisons at different damage levels.

### *3.3 Single step ahead state forecasting*

Figure 9 shows the comparison between single step ahead forecasted state and actual damage state (or damage index) with on-line data available up to the previous damage level. As seen in the figure, the prognosis algorithm starts predicting from

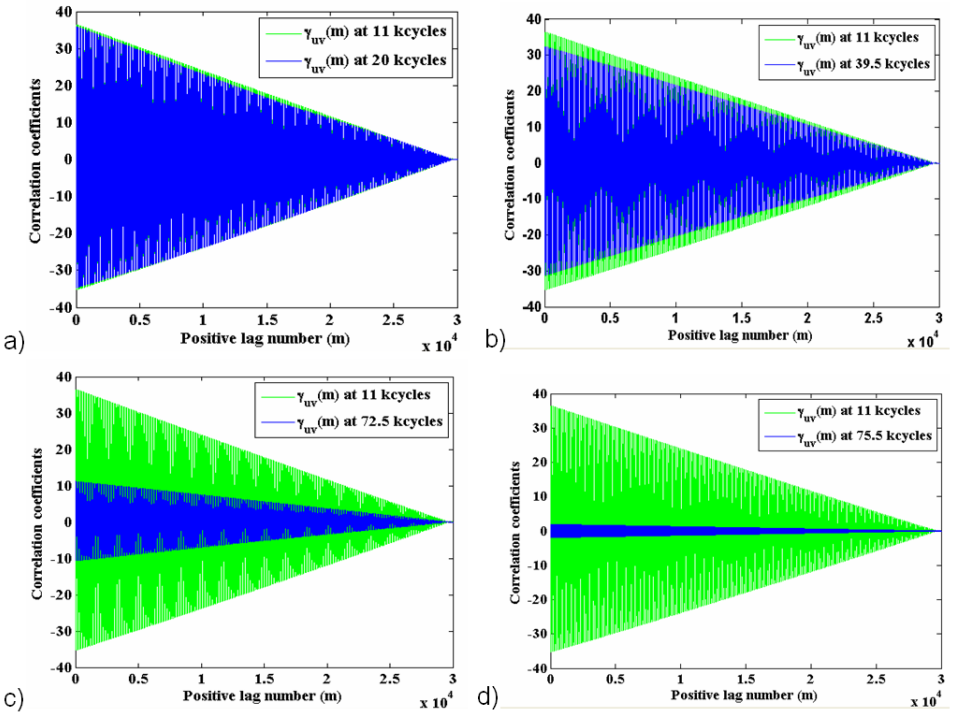


Figure 6: Cross-correlation coefficient comparison at different damage levels with the reference level at 11 kcycles

damage level 7. It is to be noted that the dimension $d$ of the Gaussian process input was chosen as 6. Therefore the prognosis algorithm requires at least six damage states to obtain the $1 \times 6$ test input vector (see Eq. 18). Also, with unavailability of any training data set $D$ (Eq. 17), to predict the $7^{th}$ damage state, the initial hyperparameters (Eq. 16) are chosen as: $\theta_n^p = \theta_n^w = 1$ and $\theta_n^{\vartheta} = 0.1$. Because of this, there is a large mismatch between the $7^{th}$ level predicted damage index and the actual damage index. However, for predicting states of damage level eight and beyond, the training input data matrix (Eq. 17) and target vectors (Eq. 18) are recursively updated. For each recursive updating, a new set of hyperparameters were obtained using the conjugate gradient optimization method. Once the hyperparameters are estimated, the one-step ahead damage index was predicted for the immediate ahead damage level. Figure 9 shows a clear correlation between one-step ahead predicted damage index and the actual damage index. It must be noted that the actual damage indices are the on-line damage states (or damage index); those were directly

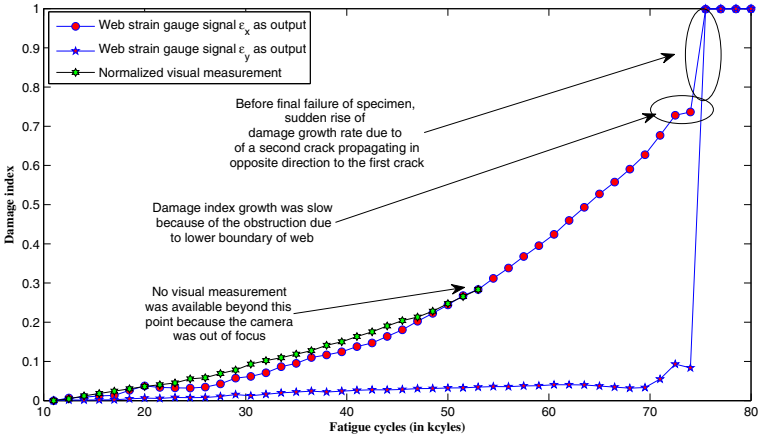


Figure 7: Variation of damage index with fatigue cycle. Flange (x-axis) strain measurements were used as input and web (x and y-axis) strain measurements as output

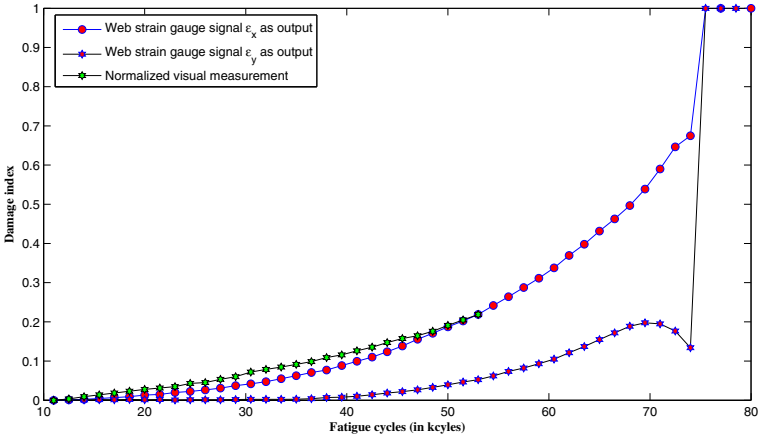


Figure 8: Variation of damage index with fatigue cycle. Horizontal axis (or x axis) biaxial frame load-cell measurements as input and web (x and y-axis) strain measurements as output

estimated from the sensor signals. The threshold value of 0.7 is 70% of the final damage index value of 1. From Eq. 5 the damage index reaches its final value of 1 when there is no cross-correlation between the input $u$ and $y$. This is because the specimen undergone complete failure. It should be noted that choosing the critical damage index value of 0.7 was based on the results from previously performed similar experiments.

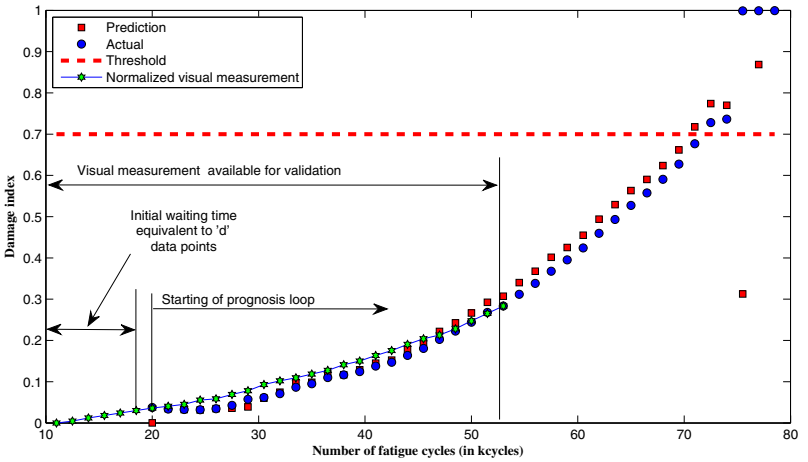


Figure 9: One-step ahead damage state prediction using off-line predictive model

### *3.4 Multi step ahead prediction*

Unlike the single step ahead prediction, the multi step ahead prediction recursively predicts the damage state multi step ahead of the damage level at which last online data was available. Figure 10 shows the multi step ahead state prediction. Similar to single step ahead prediction process, the prognosis algorithm was started after the $6^{th}$ damage level (i.e. at 18.5 kcycles). From the $7^{th}$ damage level (from 20kcycles), damage indices were predicted and then fed back to the prognosis model to update the Gaussian process training data matrix (Eq. 19) and the test input vector (Eq. 20). The feedback process and the corresponding future state predictions were continued recursively as long as the predicted damage index did not reach its critical value of 0.7. It is to be noted that unlike the single step ahead prediction, the training data matrix and the corresponding test input vector were updated with off-line model predicted states, rather than being updated with on-line model estimated states, which could not be available in real time. It can be seen from the

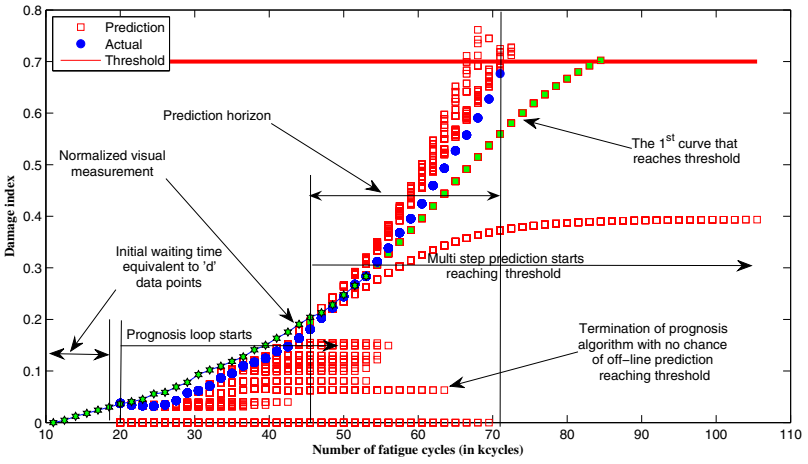


Figure 10: Multi-step ahead damage state prediction using off-line predictive model.

Fig. 10 that, with on-line data available up to damage level 23 (at 44 kcycles), the multi step ahead predicted states fails to reach the critical value of 0.7. This is because the predictive model was unable to learn the damage growth dynamics. It is also to be noted that if the predictive model does not learn the damage growth dynamics it keeps on running with only predicting unvarying damage indices. The predicted unvarying damage indices time series can also be seen from the Fig. 10. Without satisfying the threshold criteria, the prediction of unvarying damage indices could have continued indefinitely. However to reduce the computational expenses, the prognosis algorithm was stopped at certain times. The criteria for stopping the algorithm was if the rate of damage index growth was not greater than $1 \times 10^{-7}/cycles$ for six consecutive damage levels, the off-line predictive model had to be terminated. This was because of physical reason, if the damage growth was slow enough, the predicted damage index, would never reach the critical value even if the algorithm had to run indefinitely. From Figure 10 it is also seen that, the first multi step ahead prediction curve, that reaches the critical value starts from damage level 24 (from 45.5 kcycles). Beyond this damage level, the multiple step ahead prediction increasingly converges with the actual damage index. From the above mentioned observations, it can be assumed that the prediction horizon (or the true positive regime) was between damage level 24 (45.5 kcycles) and damage level 42 (72.5 kcycles), during which, the predicted damage

states reached its critical value.

### *3.5 Residual useful life estimation (RULE) and mean square error evaluation*

Using Eq. 21, the residual useful life at any given damage level (up to which the last online data was available) was estimated. Figure 11 shows the comparison of predicted RULE and actual RULE. From the figure it can be seen that, there is a good correlation between predicted and actual RULE in the true positive regime i.e., between 45.5 kcycles and 72.5 kcycles. Also as more and more online data becomes available, better correlation between predicted RULE and actual RULE is observed. Figure 12 shows the mean square error between predicted RULE and estimated RULE. It can be seen that during the true positive regime, the mean square error is substantially lesser value compared to the mean square error during the false positive regime.

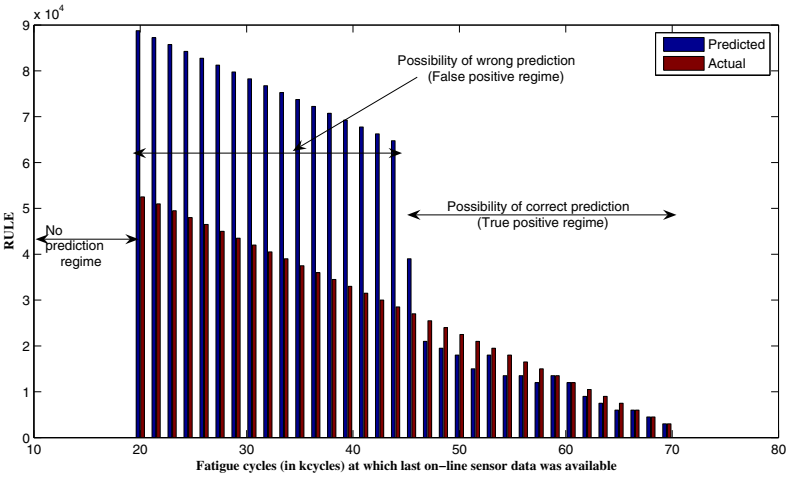


Figure 11: Comparision of predicted RULE and actual RULE.

## 4 Conclusion

An on-line-off-line prognosis model is proposed for adaptive future damage state prediction and residual useful life estimation. The proposed prognosis model combines an on-line state estimation model with an off-line predictive model to adaptively estimate the residual useful life of an Al-6061 cruciform specimen under biaxial loading. The on-line model was based on a correlation analysis approach,

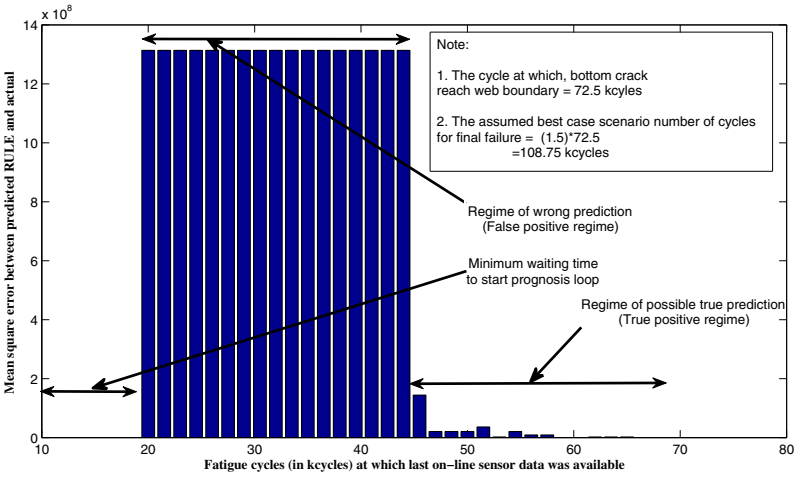


Figure 12: Mean square error between predicted RULE and actual RULE.

which estimates the current damage states. The numerical results showed good correlation between on-line estimated state and the normalized visual measurements. Once the current damage state was available from the on-line model, the information was fed to an off-line predictive model to obtain the future states and remaining useful life estimation (RULE). The off-line predictive model is a high-dimensional kernel function based recursive Gaussian process model. The future states are recursively predicted by feeding back the previous predicted states to the off-line model. Also, the model parameters (Gaussian process hyperparameters) were updated with repetitive conjugate gradient based optimization. Good correlation was also observed between actual damage states and predicted future damage states well before the final failure occured. Furthermore, a good correlation between predicted RULE and actual RULE is also observed during which, the predicted damage index reached its critical value.

**Acknowledgement:** This research was supported by the MURI Program, Air Force Office of Scientific Research, and grant number: FA9550-06-1-0309; Technical Monitor, Dr. David S Stargel.

## References

**Billington, S.; Zhang, C.; Kurfess, T.; Danyluk, S.; Liang, S.** (1999): Adaptive prognostics for rolling element bearing conditions. *Mechanical Systems and Signal Processing*, vol. 13, pp. 103–113.

**Farrar, C. R.; et. al.** (2003): Damage Prognosis: Current Status and Future Needs. Technical Report LA-14051-MS, Los Alamos National Laboratory, Los Alamos National Laboratory, USA, 2003.

**Farrar, C. R.; et. al.** (2007): Nonlinear System Identification for Damage Detection. Technical Report LA-14353, Los Alamos National Laboratory, Los Alamos National Laboratory, USA, 2007.

**Gibbs, M. N.** (1997): Bayesian Gaussian Processes for Regression and Classification). Technical Report PhD Thesis, University of Cambridge, Dept. of Physics, University of Cambridge, U.K, 1997.

**Gupta, S.; Ray, A.** (2007): Real-time fatigue life estimation in mechanical structures. *Meas. Sci. Technology*, vol. 18, pp. 1947–1957.

**Harter, J. A.** (2003): AFGROW Users' Guide and Technical Manual. Technical Report AFRL-VA-WP-1999-3016, AFRL, Air Force Research Laboratory, USA, 2003.

**Iyyer, N.; Sarkar, S.; Merrill, R.; Phan, N.** (2007): Aircraft life management using crack initiation and crack growth models - P-3C Aircraft experience. *Int. J. of Fatigue*, vol. 29, pp. 1584–1607.

**Liu, Y.; Mahadevan, S.** (2007): Stochastic fatigue damage modeling under variable amplitude loading. *Int. J. of Fatigue*, vol. 29, pp. 1149–1161.

**Ljung, L.** (1999): *System Identification: Theory for the User*. Prentice-Hall, Cambridge, MA.

**MacKay, D.** (1992): Bayesian Interpolation. *Neural Computation*, vol. 4, pp. 415–447.

**MacKay, D.** (1998): *Introduction to Gaussian Processes, Neural Networks and Machine Learning*. Springer, Berlin.

**Mohanty, S.; Chattopadhyay, A.; Peralta, P.** (2008): On-line Life Prediction of a Structural Hot-Spot. *ASME Conference on Smart Materials, Adaptive Structures and Intelligent Systems, October 28-30, Ellicot City,MD*.

**Mohanty, S.; Das, S.; Chattopadhyay, A.; Peralta, P.** (2009): Gaussian Process Time Series Model for Life Prognosis of Metallic Structure. *Journal of Intelligent Material Systems and Structures*, vol. 20, pp. 887–896.

**Neal, R. M.** (2003): Probabilistic Inference Using Markov Chain Monte Carlo Method. Technical Report CRG-TR-93-1, University of Toronto, Dept. of Computer Science, University of Toronto, Canada, 2003.

**Newman, J. C.** (1992): FASTRAN-II - A Fatigue Crack Growth Structural Analysis Program. Technical Report NASA Technical Memorandum 104159, NASA Langley Research Center, NASA Langley Research Center, USA, 1992.

**Rasmussen, C.; Williams, C.** (2006): *Gaussian Processes for Machine Learning*. MIT Press, Cambridge, MA.

**Williams, C.** (1997): In *Advances in Neural Information Processing Systems*. MIT Press.

**Wu, W. F.; Ni, C. C.** (2004): Probabilistic models of fatigue crack propagation and their experimental verification. *Probabilistic Engineering Mechanics*, vol. 19, pp. 247–257.